RESEARCH

Glass–ceramic foams from waste glass and natural red soil

Amel Sadji[1] · Mohamed Redda Boudchicha[1,2] · Aicha Ziouche[3] · Abdelkader Filali[4,5] · Slimane Achour[1]

Abstract

In this study, waste glass obtained from a discarded green glass bottle and unexploited natural red soil (RS) were prepared to get glass–ceramic foams. Red soil is an earthy material, which is used as a foaming agent. A mixture of starting powders containing different mass fractions (5–16 wt.%) of RS with particle size smaller than 20 μm was uniaxially pressed (at 30 MPa), and the obtained compacts were fired at different temperatures (750–850 °C) and holding time (30–120 min). Furthermore, the influences of temperature, holding time, and natural rock additions on the structure, type, and size of pores, besides physical and mechanical properties of the processed foamed glass–ceramic samples, were investigated. The results show that the optimum foaming temperature was found to be 800 °C leading to a maximum value of porosity as high as 90%, while the bulk density and compressive strength reached the values 0.26–0.75 g·cm^{-3} and 1.2–6.1 MPa, respectively. Based on the present data, the obtained glass–ceramic allowed the preparation of different porosity types. Therefore, they provide practical value for specific applications where thermal insulation is desired.

Keywords Porous materials · Waste glass · Calcium carbonate · Glass–ceramics · Foams

Introduction

Glass is one of the most used materials globally; it is widely used for various applications such as lighting, buildings, and packaging, due to its excellent properties [1]. In recent times, the rapid development of technology led to a diminution in natural resources and increased industrial, household, and commercial waste.

Billions of tons of discarded glass are abandoned and thrown in nature each year. Its presence can cause real danger and severe environmental pollution. As glass is non-biodegradable, several scientific studies have been interested in applying modern technologies to waste glass. Recycling thus becomes a necessary option to save energy in manufacturing, reduce natural resource consumption, and minimize the impact of waste on the environment. Currently, many researchers suggest the possibility of converting glass powders into advanced materials such as glass–ceramics [2], ceramic bricks [3], lightweight concrete [4], and porous materials [5]. Therefore, the progress of new porous materials produced by recycling glass waste acquired a great interest in the construction sector, especially in terms of mechanical properties and structural applications.

Glass foams are a porous material with porosity usually higher than 60%. They can be produced with open and/or closed structures [6]. Its excellent proprieties, such as low thermal conductivity, low density, permeability, and high surface area [7], make glass foam a competitive and interesting material for many applications in many fields, mainly for thermal and sound insulation materials [8]. Usually, all-glass foams are produced by the powder method. Among the various techniques that have been applied and cited in the literature are gel casting [9], replica [10], and the incorporation of blowing agents [11]. The direct foaming technique is the most frequently used

✉ Abdelkader Filali
f.abdelkader@imperial.ac.uk

1   Laboratoire de Technologie Des Matériaux Avancés, Ecole Nationale Polytechnique de Constantine, BP75, A, 25000 Nouvelle Ville Ali Mendjli, Constantine, Algeria

2   Laboratory of Physical and Chemical of Materials (LEPCM), University of Batna 1, Batna, Algeria

3   Research Center in Industrial Technologies CRTI, Cheraga, P.O. Box 64, 16014 Algiers, Algeria

4   Laboratoire de Mécanique Et Systèmes Energétiques Avancés, Ecole Nationale Polytechnique de Constantine, BP75, A, 25000 Nouvelle Ville Ali Mendjli, Constantine, Algeria

5   Chemical Engineering Department, Imperial College London, South Kensington Campus, London SW7 2AZ, UK

approach due to its simplicity. It consists of integrating a foaming or pore-forming agent in small quantities, such as fly ash [12], tobacco residue [13], banana leaves [14], and eggshells wastes [15], in a glass powder (cullet).

The cellular structure can be realized by adding suitable substances (blowing agents) that generate gaseous product during continuous heating. The foaming agent is classified as a neutralization and redox agent. Neutralizing agents are usually carbonates [16] or sulfates such as $CaCO_3$, Na_2CO_3 [11], dolomite ($MgCa(CO_3)$ [17]), or organic compounds. Upon heating, the carbonate particles decompose, releasing CO_2 gas. The gaseous product is trapped in the molten glass to produce foamed glass inside which sealed pores prevail. The product of the reaction, for example, CaO or Na_2O, is incorporated into the glass and acts as a modifier that affects the viscosity and properties of the glass, while redox agents, such as carbon-containing materials like sugar, Si_3N_4 [18], SiC, and pure carbon [19], pass through an oxidation reaction by gases dissolved in the softened glass mass, such as oxygen-forming gaseous products of CO_2 or CO.

The selection of the sintering temperature is crucial for the foaming process, as the glass viscosity and the foaming temperature are strictly related. The initial size of the starting powder, the heating rate, the heat treatment time, and the amount of added foaming agent must be precisely controlled. These parameters are necessary to optimize the final product and control the structure of the porous glass [20].

Many researchers have identified calcite as a critical raw material. Considering this aspect, finding alternative sources to fabricate glass foam is essential. Furthermore, the valorization of natural residues opens many economic opportunities and can be a low-cost alternative for use as foaming agents in producing value-added materials. In this regard, a natural red soil (RS) extracted from the local region very abundant (Constantine, Algeria), rich in calcium carbonate $CaCO_3$, has been employed as a pore-forming agent (foaming agent), due to the emissions of CO_2 gases after the heating process. Red soils are defined as marl rock and may be found in arid, semiarid, and even some humid climate environments, a compound composed primarily of calcium carbonate and a variable percentage of noncrystalline clay. Red soils generally have a wide range of characteristics and technical properties. The presence of calcium carbonate plays an essential role in the durability of the soil and its chemical and physical properties. This source is used because of its low price, high yield, and abundance [21–23].

This work aims to lower the foaming temperature for producing porous glass–ceramics from green bottle waste and red soil rich in calcium carbonates and promoting
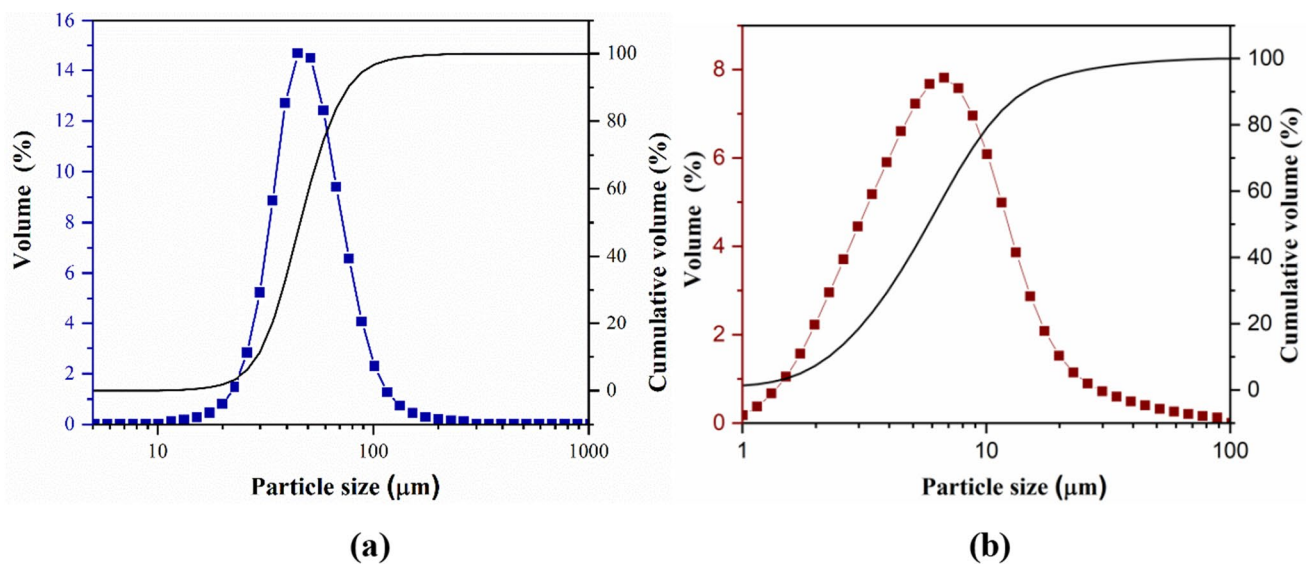

Fig. 1 Particle size distribution of **a** the glass powder and **b** natural red soil (RS)

Table 1 Chemical composition of GB glass and red soil (RS)

Raw materials	Constituent oxides (wt.%)								
	SiO_2	CaO	Fe_2O_3	Al_2O_3	MgO	SO_3	K_2O	Na_2O	LOI
GB glass	70.07	14.89	0.50	2.02	0.89	/	/	11.60	0.03
RS	14.5	46.74	1.67	2	0.57	0.11	0.14	0.1	34.17

homogeneous microstructure using a smaller particle size. Several samples are developed to study the impact of foaming agent concentration (5–16 wt.%), foaming temperature, and heat treatment time on physical, mechanical, and structural properties for various applications such as insulation.

Materials and methods

Raw materials

The waste glass is gathered from discarded green glass bottles (GGB); natural red soil (RS) extracted from the local region was used as a pore-forming agent (foaming agent) (Fig. 2). In general, two types of clays, called calcareous clays (Ca-rich clays) and noncalcareous clays (Ca-poor clays), are found in soil. Both can contain kaolinitic and illitic clays with free quartz as a major impurity [24, 25].

Sample preparation

The sample preparation process started with cleaning the recovered glass bottles under a fixed temperature of 100 °C for 12 h. Then, these bottles were crushed using a hammer and subsequently ball-milled until achieving a particle diameter of 40 meshes (< 500 microns). Next, a planetary mill (Retsch, PM100) was used for 2 h at 300 rpm to dry process each. Finally, a glass powder with a particle size < 20 μm was obtained. The natural red soil was dried at 100 °C for 24 h and subsequently fragmented and crushed, using a hand mortar, into a fine powder.
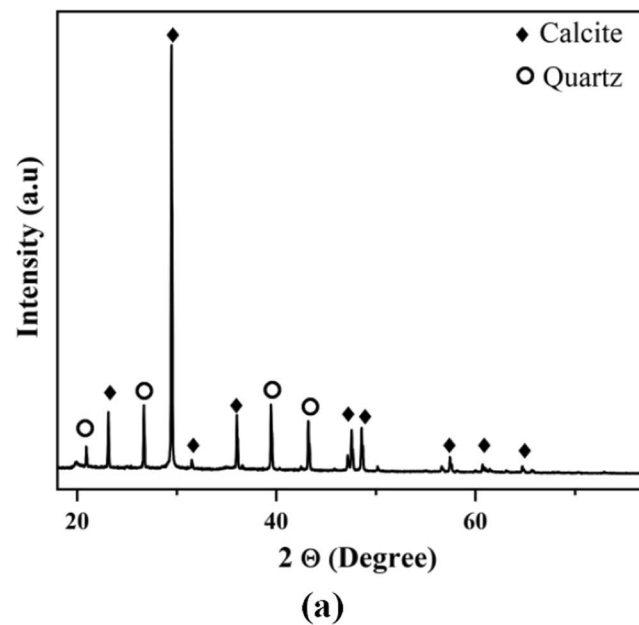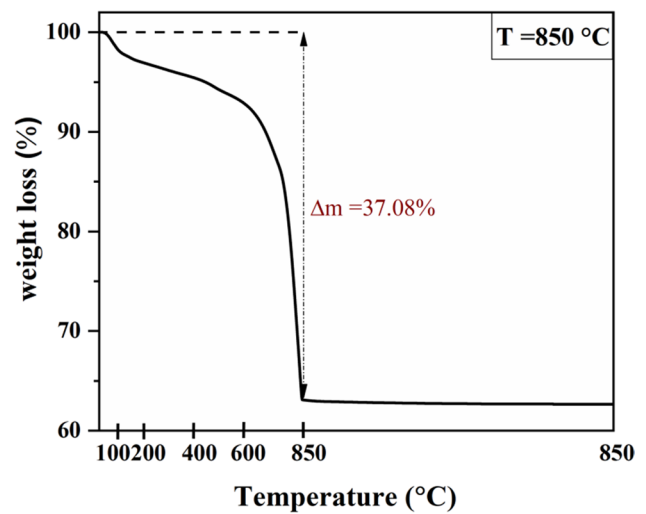

Fig. 3 Weight loss of natural red soil (RS)

To obtain the glass–ceramic foam, different proportions of GGB ((wt.%)/RS (wt.%): 95/5, 90/10, 87/13, and 84/16) (the samples were named G5, G10, G13, and G16, respectively) were prepared by wet mixing and discs of 13 mm diameter and 4 mm thick were obtained, after drying (100 °C/24 h) by uniaxial compression.

Characterization techniques

The mean particle size distribution of the raw materials after grinding was obtained by the Laser Scattering Particle Size Distribution Analyzer LA-960V2. An X-ray fluorescence

Fig. 2 XRD Pattern of **a** natural red soil (RS) and **b** the glass powder
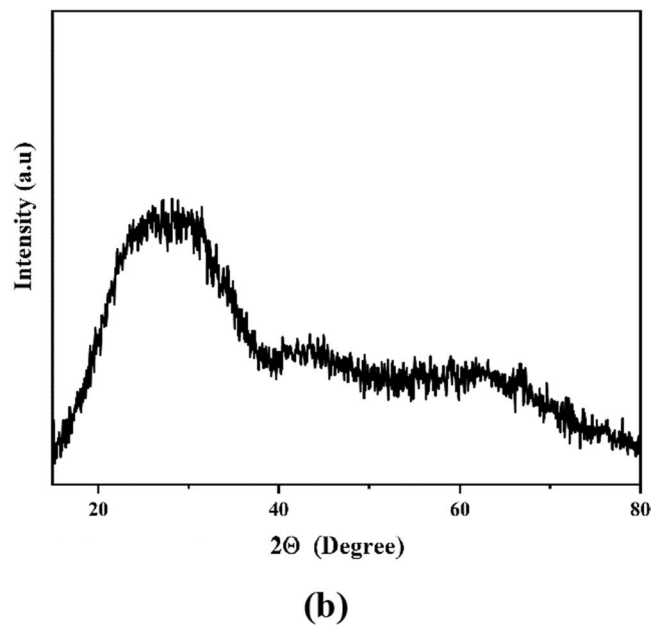
spectrometer (Epsilon 3 XL, PANalytical) was used to analyze the chemical composition of the starting materials. To determine amorphous and crystalline phases of powders and fired samples, X-ray diffractions were performed by XRD diffractometer (Philips, X'Pert), using Cu Kα radiation at 40 kV, 35 mA, with a step width of 0.02° ranging from 15° to 80°. ICDD cards were used to identify peak intensity and position.

The thermal measurement of powder was performed using thermogravimetric (TG) analysis (METTLER TOLEDO, TGA 2) in the air between 20 and 880 °C at 10 °C/min. First, the foam samples' bulk density (ρ_b) was computed based on their geometrical dimensions (measured by a caliper) and their masses. Then, the true density (ρ_t) of powder samples was measured using a gas pycnometer (Micromeritics Accupyc 1340). Finally, the total porosity (p) was estimated using Eq. (1) from the true and bulk densities:

$$p = \left(1 - \frac{\rho_a}{\rho_t}\right) * 100\% \tag{1}$$

The volume expansion was calculated from the following equation:

$$V = \frac{V_f - V_i}{V_i} \tag{2}$$

where V_i and V_f denote the initial and final volumes of the glass foams, respectively. Each data point was obtained as the mean value of at least 4 individual measurements. The size, shape, and distribution of the pores in the fired foams were determined using optical microscopy (Novex Stereo Microscope AP 8).

To compute and verify the mechanical strength of the glass foams, the compression stress was applied to a cube with nominal dimensions of 10 mm × 10 mm × 10 mm; each specimen
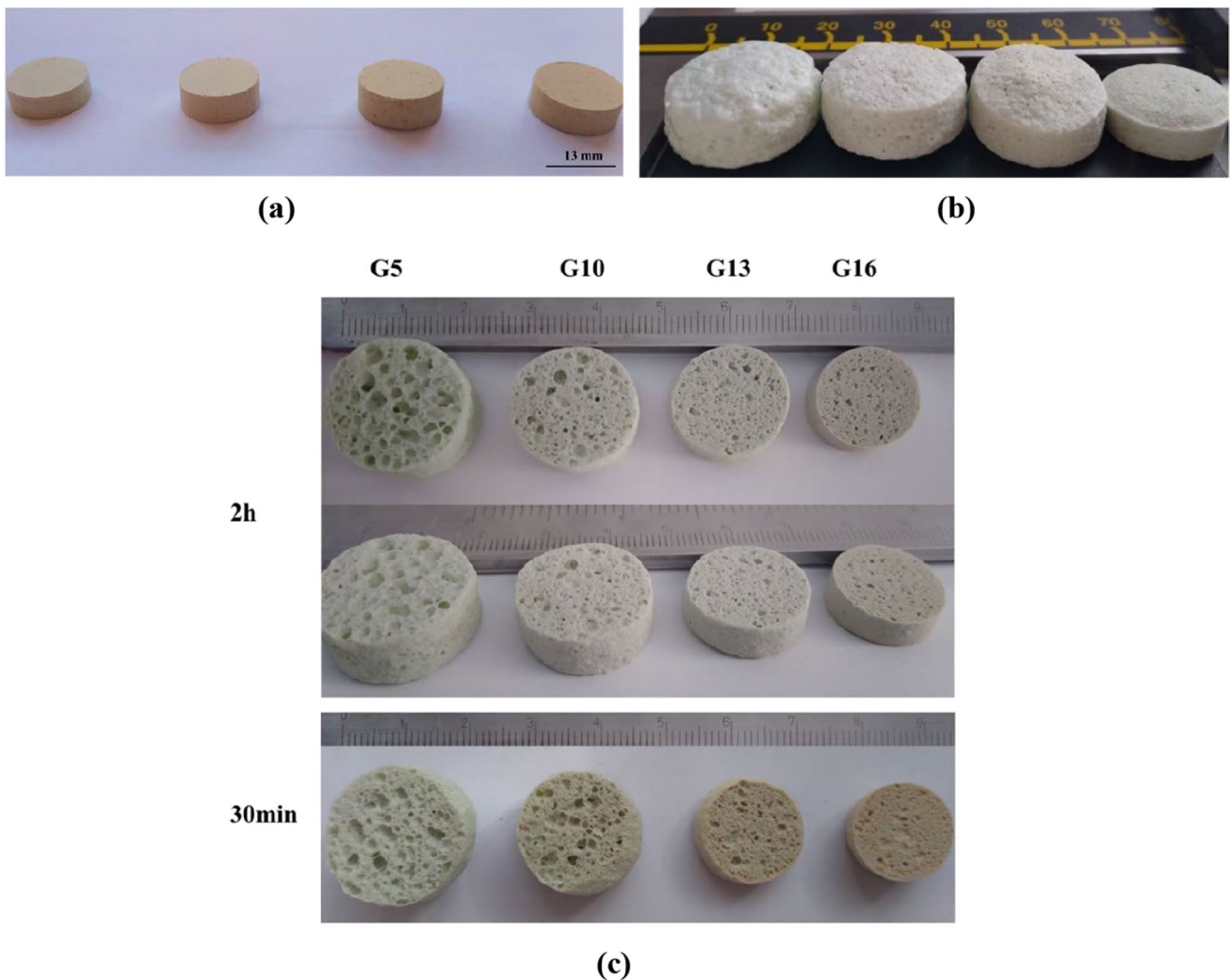

Fig. 4 **a** Top view of the green sample. **b** Effects of the content of RS on the foamed-glass samples. **c** Top and side views of samples G5, G10, G13, and G16 fired at 800 °C for 30 min and 2 h
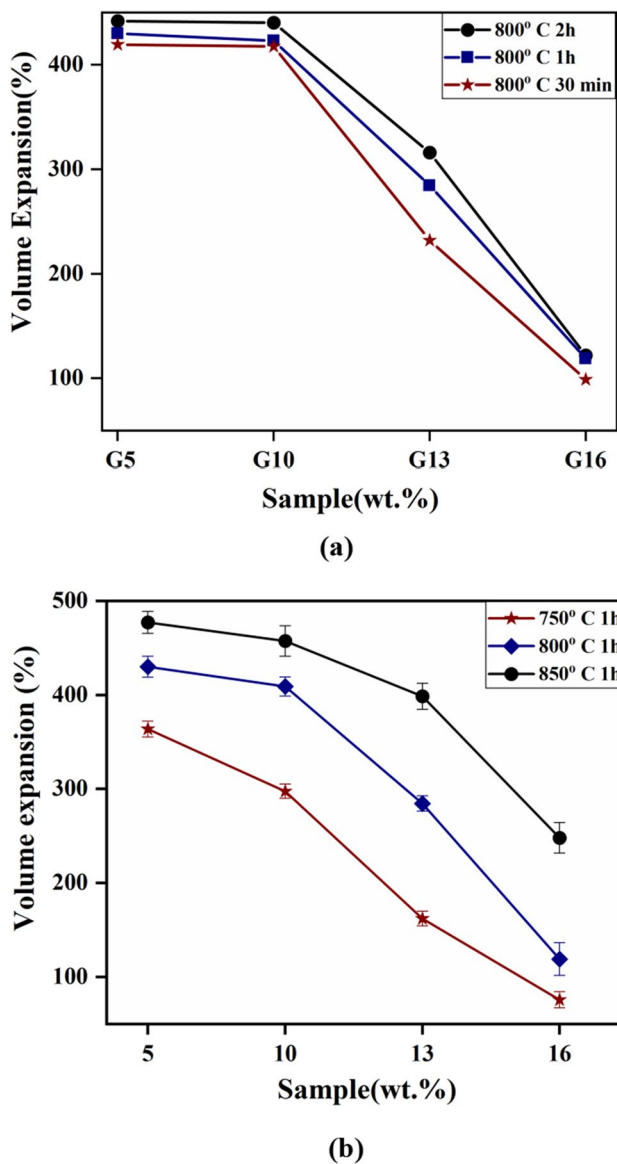
Fig. 5 Variation of volume expansion with different contents of red soil fired at **a** 800 °C with different holding times and **b** 750 °C, 800 °C, and 850 °C for 1 h

was cut from porous material using a hacksaw and refined with abrasive paper before being loaded onto a universal machine (Lloyd-Ametek, EZ2) at a loading speed of 0.5 mm·min^{-1}. Images of fired samples using a scanning electron microscope SEM (Tescan Vega3) revealed the microstructure and morphology of the pores.

Results and discussion

Compositions of raw materials and characterizations

Figure 1a, b illustrates the particle size distribution of raw materials after the milling process. The cumulative curves

exhibit a monomodal distribution, with an average size (*D*50) of about 12.55 μm for the glass powder (90% of the particle size have sizes smaller than 20 μm) and *D*50 of 5.7 μm for the natural red soil (90% of the particle size have sizes smaller than 14 μm).

The results of the chemical analysis of the starting materials obtained by XRF are shown in Table 1. The composition of green glass bottles (GGB) is typical of the silica-soda lime glass family, with SiO$_2$ being the most important element. Besides substantial amounts of calcium oxides and sodium, the presence of iron oxide is due to the green coloration of the bottle [26]. Otherwise, the red soil used as a pore-forming agent is mainly composed of calcium carbonate (CaCO$_3$) (46.74 wt.%) and silicon oxide (SiO$_2$) (14.5 wt.%). Aside from these oxides, the existence of iron oxide, aluminum oxide, sodium, and magnesium is also observed. Sodium and magnesium can be found in the form of carbonate; since the LOI is very high. The mean values of these analyses indicate that the used soil is mainly composed of red clay and calcium carbonates. The red color is due to the presence of iron oxide.

The XRD pattern of RS and waste glass is displayed in Fig. 2. The XRD of the RS sample (Fig. 2a) reveals the presence of calcium carbonate and CaCO$_3$ (PDF 01–083-0578) as the major phase, also the presence of a silica phase, the quartz-type (SiO$_2$) (PDF01-087–2096). The presence of calcium carbonate (CaCO$_3$) in the RS sample is very interesting for this study. According to the literature, this phase is an agent of pore formation [15, 26–29].

The XRD results of the glass powder showed a typical amorphous soda-lime glass structure.

Intending to study the thermal transformations and the effects of natural red soil (RS) on the mixture and proprieties of glass foam, the thermogravimetric analysis (TGA) was investigated between 25 and 850° C. This analysis is essential because it reveals the weight loss, the beginning of the pore formation process, and the temperature at which gases are formed.

Figure 3 presents the mass loss from the TGA of the blowing agent. It was found that a continuous weight loss starts at about 100° C and reaches a maximum value at 850 °C; beyond this temperature, there was no more calcium carbonate decomposition, resulting in a total loss of 37.08%. So, the carbonate substances investigated here show that the RS mineral emits enough amount of CO$_2$ gas to cause the expansion of a soda-lime glass at its softening temperature by creating vitreous. In addition, a gas formation from kaolinite in the kaolinitic clay decomposition at about 600 °C may contribute to the observed foaming effect at relative temperatures (530–650 °C).
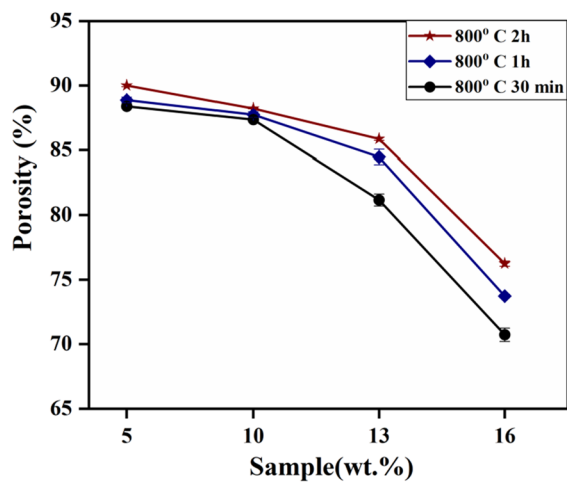
To identify the temperature at which the pore-foaming processes can take place, information on the glass transition, foaming temperature, and viscosity is required.
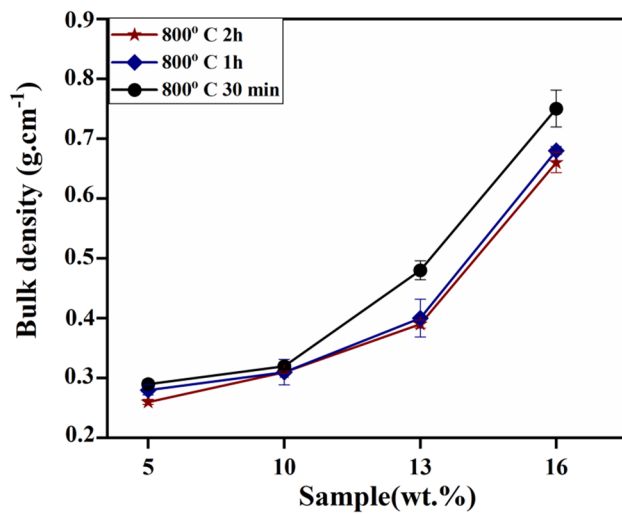
(a)
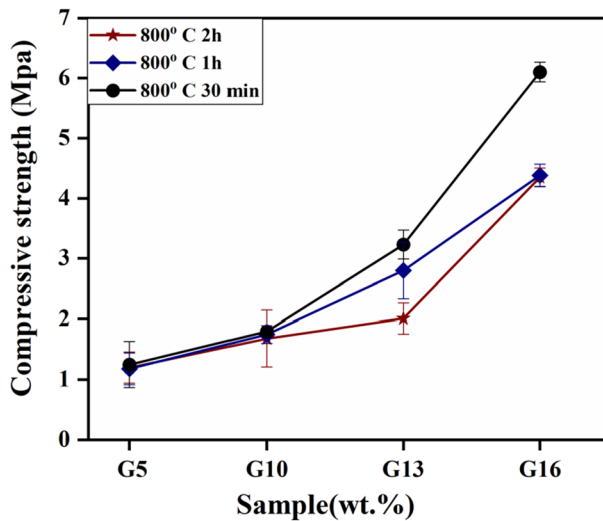
(b)

(c)

Fig. 6 Effects of RS content and holding time on **a** bulk density, **b** compressive strength, and **c** porosity of samples heated at 800 °C
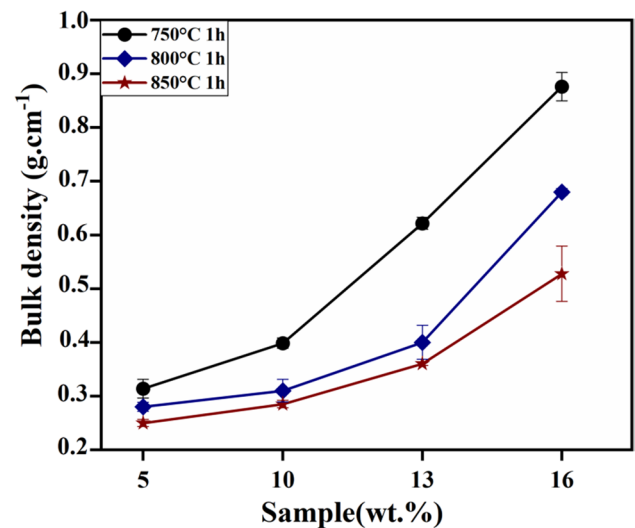

Fig. 7 The bulk density for various samples and different sintering temperatures on the bulk density

The SiO_2 content determines the softening point of glass. As reported in the literature, soda-lime glasses with 60 wt.% and 80 wt.% of SiO_2 have softening temperatures of 820 °C and 630 °C, respectively. In this study, the softening point is approximately ($T = 700$ °C). It is noted that the most suitable viscosity range for gas generation is between 10^3 and 10^5 p.a.s (800 and 1000 °C) [30]. In our case, this is referred to as the operating range. In fact, the decomposition of carbonate and the formation of initial pores starts from 650 °C before the softening of the glass matrix; the gases generated from initial pores can increase via the gas-expanding process and reduce the glass viscosity by increasing the temperature. The continuous pore development results from the pore's internal pressure increase against the matrix. Furthermore, temperatures greater than 750 °C are necessary due to the usage of the maximum quantity of gases and the development of the expansion mechanism. As a result, 800 °C was chosen as the sintering temperature in this study.

Physical and mechanical analysis

Effect of blowing agent content and holding time

To investigate the evolution of physical and mechanical properties, volume expansion, porosity, bulk density, and compressive strength were studied.

The evolution of volume expansion and the top view of foamed glass samples as a function of heat treatment temperature, different foaming agent content, and holding time are shown in Figs. 4 and 5.

Before firing, the green samples have a cylindrical shape (Fig. 4a). From Fig. 4b, it can be observed that the shape
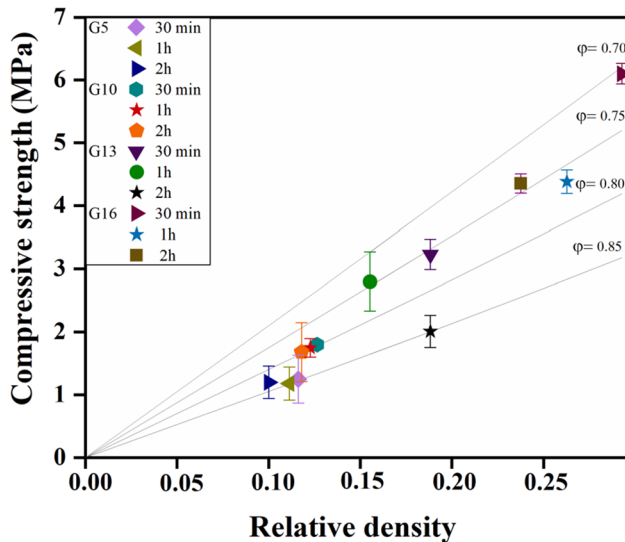
Fig. 8 The compressive strength versus the relative density of the foam glass fired at 800 °C

and volume of the expanded samples prepared under various conditions changed from a cylindrical to a barrel form that is dense and crack-free. Figure 4c shows that the volume declines with the rise in the RS content and that the diameter of the internal pores gradually decreases. However, the increase in the sintering time leads to an increase in the volume and diameter of the glass foam.

Figure 5a, b shows that the volume expansion significantly differs between 5 wt.% and 16 wt.% RS. The maximum value obtained from 5 wt.% RS was 477.13%, while the minimum volume expansion was 75.65% from 16 wt.% RS.

The volumetric expansion is much lower at 750 °C, which can be explained by the lowest RS decomposition rate confirmed by mass loss in ATG thermal analysis. The volume starts to increase from this temperature and reaches a maximum of 850 °C.

The porous ceramics elaborated with 16 wt.% RS and sintered at 800 °C for 120 min are the most expanded compared to the samples fired at the same temperature during 30 min. The maximum expansion was achieved when 5 wt.% was added to green powder fired during 120 min.

The effects of holding time and the different contents of RS on the porosity, bulk density, and compressive strength for glass–ceramic foams sintered at 800 °C are plotted in Fig. 6.

According to this figure, increasing the foaming agent content increases the compressive strength and the bulk density while decreasing the porosity. For instance, increasing the amount of red clay in the green sample from 5 (wt.%) to 16 (wt.%) and sintering at 800 °C for 1 h result in a significant increase in the bulk density from 0.28 g/cm^3 to 0.68 g/cm^3 and the compressive strength from 1.18 MPa to 4.38 MPa. Nevertheless, these increases accompany a porosity decrease from 88.87% to 73.72%. So, sample G5 has the highest porosity. Therefore, the effects of RS content might be expressed in terms of viscosity.

The variation of the glass viscosity versus the temperature is provided by the Fucher [31] Eq. (3):

$$\log\ n = -A + \frac{B}{T - T_0} \tag{3}$$

where T is the temperature and n is the viscosity. A, B, and T_0 are characteristic constants which vary regularly with the composition.

According to the literature, the change in log n is proportional to the percentage of CaO substituted. The difference in bulk density and porosity values is most likely due to changes in surface tension and viscosity of the glass melt upon the addition of CaO from the decomposition of the foaming agent. The change of the glass viscosity, in particular, relies on the miscibility of the oxide system [31]. Taking into account these considerations, the sample containing 5 wt.% of RS can be assigned to the lowest softening temperature. The low softening temperature causes a minor degree of phase separation, and the drop in bulk density is attributable to carbonate decomposition and CO_2 generation during the foaming process. Sample G10, on the other hand, contains more RS (10 wt.%). So, it should have a higher viscosity, leading to more remaining gas in the sample, resulting in more closed pores and higher porosity. However, by adding more foaming agents in G13–G16, the molten glass will have a low surface

Table 2 Comparison between the physical and mechanical proprieties for the sample heated at 800 °C and some results obtained from the literature

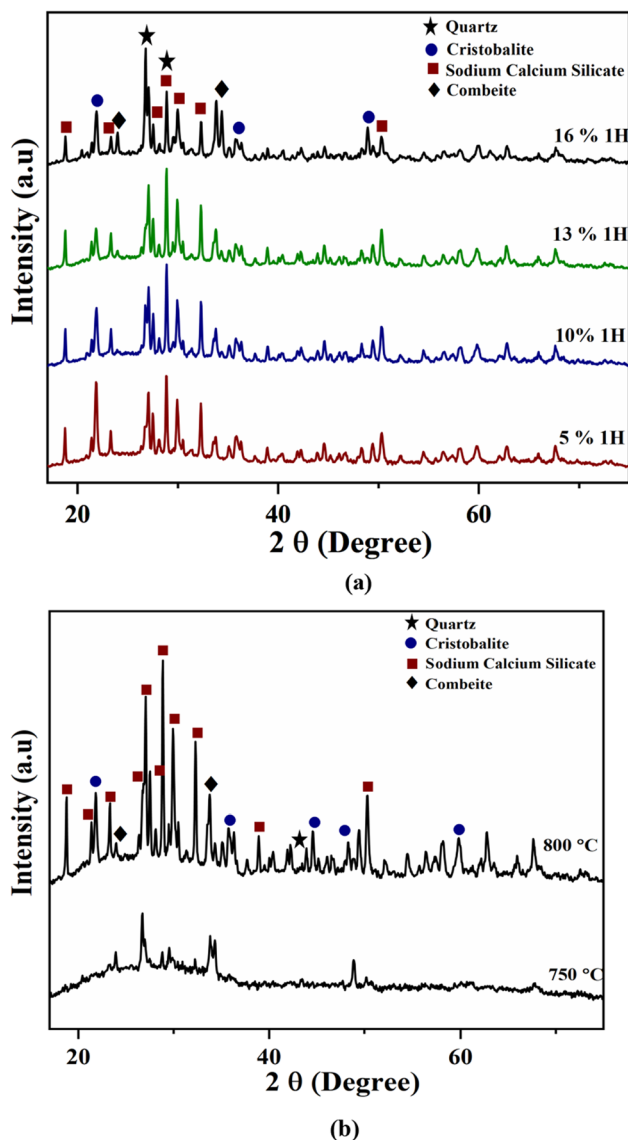| Glass content	Foaming agent	T(°C)	ρ_a (g/cm^3)	P_t (%vol)	σ(MPa)	Ref
Glass bottles	Red soil	800	0.26	90	1.2	This work
			0.75	70	6.1	
Glass bottles	Eggshells	900	0.5	83	1.50	[26]
			0.5	83	1.50	
Glass bottles	Banana leaves	700	0.4	85	2.2	[14]
Glass bottles	Banana leaves	800	0.32	88	1.1	[14]
SLS glass	Eggshells	800	0.421	83.6	0.42	[15]

Fig. 9 XRD analysis of foam samples after firing for 60 min **a** at 800 °C with different foaming agent contents and **b** at 750 and 800 °C containing 13 wt.% RS

tension because of the lower liquid phase and higher viscosities. This will hinder the growth of pores and the generated gas flow. As a result, these samples have a lower porosity than G5 and G10.

Also, the density of glass foam depends strongly on the holding time because it is necessary to optimize the time for the reaction of the pore-forming agent to be completed. As can be seen, the bulk density declines while the porosity rises with the prolongation of the duration of heat treatment. During the period of gas release, the density reached a minimum value with a time of 120 min. When this step is completed, a gradual foam breakdown and collapse via coalescence of the pores begin [7]. According to the graphs shown in Fig. 6, a

good correlation between bulk density and compression strength can be observed, although it was indirectly proportional to the porosity.

Effect of heat treatment temperature

The samples G5–G16 were fired at different temperatures from 750 to 850 °C; the evolution of bulk density is shown in Fig. 7. Generally, as the temperature increases, the bulk density declines with the temperature increase. At $T = 750°C$, the bulk density achieved a maximum value since the foaming process occurred with the growth of gas bubbles due to the relatively high viscosity of the gas phase and the partial decomposition of calcium carbonate. As the heat treatment temperature reaches 800 °C, the viscosity of the liquid glass phase is reduced, leading to the generation of the liquid phase, which is favorable to the sintering process. Also, the decomposition reaction of the foaming agent intensifies the gas pressure and bubbling, promoting the swelling of pores. Consequently, the produced CO_2 gas becomes more challenging to evacuate, resulting in the formation of larger closed pores.

To understand the mechanical behavior of highly porous ceramics, Gibson and Ashby (GA) have proposed their theories. The deformation behavior of porous materials can be interpreted from three dominating factors: the cell shape, the relative density, and the properties of the solid.

The mechanical strength of glass foams is meanly determined by the relative density and microstructure (closed or open porosity). Figure 8 shows the relationship between relative density and compressive strength.

The classical model for the collapse stress of cellular structural materials proposed by Gibson and Ashby [32] presents the dependency of compressive strength (σ_c) on the porosity (p) as follows

$$\sigma_c = \sigma_{bend}\left[C(\varphi\rho_{real})3/2 + (1 - \varphi)\rho_{real}\right] \qquad (4)$$

where ρ_{real}, σ_{bend}, φ, and C are, respectively, the relative density of the glass foam (the ratio of bulk density to powder density), the bending strength of the used glass (typically given as 70 MPa) [33], the correction factor, and a dimensionless constant equal to 0.2 [32].

From Eq. (4), the first term is due to bending and the second term is due to membrane stretching of the cell walls. The quantity $(1 - \varphi)$ represents the volume fraction of solids laying in the cell walls and their contribution to the cell's mechanical strength. For a closed-cell foam, $\varphi = 0(1 - \varphi = 1)$, with the solid phase constitutes mostly cell walls and thus enhancing the linear term, whereas if the foam is open-celled, the pores are fully interconnected with material only on the cell edges, then $\varphi = 1(1 - \varphi = 0)$.

From Fig. 8, we can see that the compressive strength depends mainly on the relative density (i.e., it decreases with
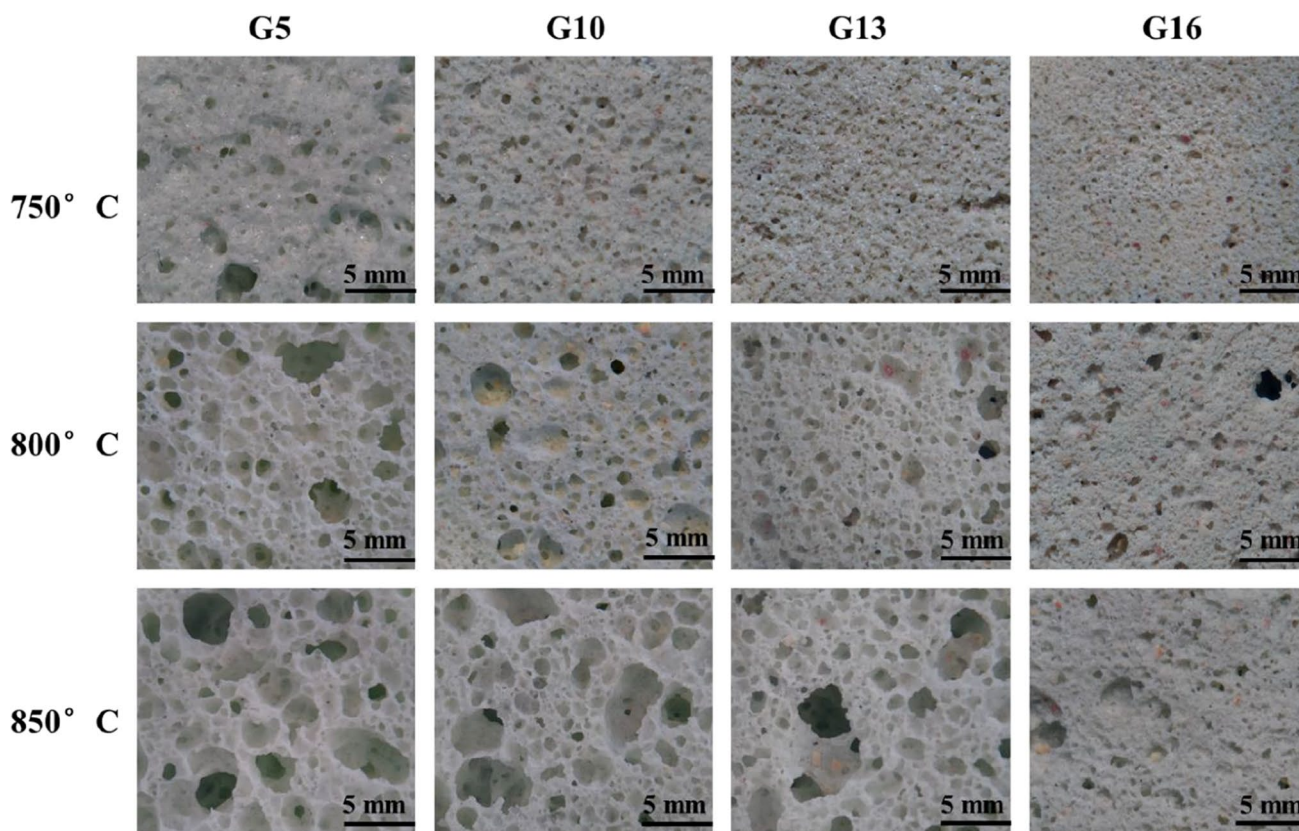
Fig. 10 Microstructure of samples foamed with different concentrations of red soil sintered at different heat treatments for 60 min

increasing relative density). As we will see later, density is not the only parameter affecting the pores' strength and morphology. Therefore, we can deduce that closed porosity structures should have higher mechanical properties than open porosity structures.

The compressive strengths of the examined glass foams fit well with the values φ in the interval of 0.70 to 0.85 for the relative density range 0.10–0.29 (the density being in the range 0.29–0.75 g/cm^3). This result indicates that φ values decreased with the increase of relative density, which envisages a tendency for the foams to change from open-celled to the closed-cell structure.

It is obvious that the most homogeneous samples, fired for 30 min, can be considered the best since they represent the most remarkable compressive strength and specific strength (strength-to-density ratio), while the foams fired for 120 min were still particularly strong, despite the high porosity due to the remarkable crystallization. A probable reason is that the phenomenon of coalescence of pores occurred with the increase of the holding time. For a low content of RS (5 wt.% and 10 wt.%), the relative density increases from 0.10 to 0.12 (the apparent density is in the range of 0.26–0.32 g/cm^3); the compressive strength fits well with the φ values between 0.85 and 0.8. However, by adding more foaming agents in G13 and G16, the relative density

became higher than 0.12 (the apparent density being in the range 0.48–0.75 g/cm^3), and the compressive strengths fit well with φ values less than 0.8. In addition, the specific strength shows an increase (from 4.21 to 8.13 MPa cm^3/g). The results indicate that the obtained foams are close to reported glass–ceramic foam and commercial foams [7, 18, 34–38].

From the microscopic observations and the determined fit values of φ, it can be inferred that the closed pore structures have improved mechanical properties compared to the open pore structures. This is mainly due to the strength of the faces and the high volume fraction of solids located at the cell edges. In addition, coarse microstructures with larger pores can correspond to high φ values and are more sensitive due to the small ratio of cell face thickness.

Table 2 compares the physical and mechanical proprieties for the sample heated at 800 °C and the results obtained in the literature.

Structural analysis

The XRD data were collected to identify the amorphous and/ or crystalline phases during the production of glass foam.
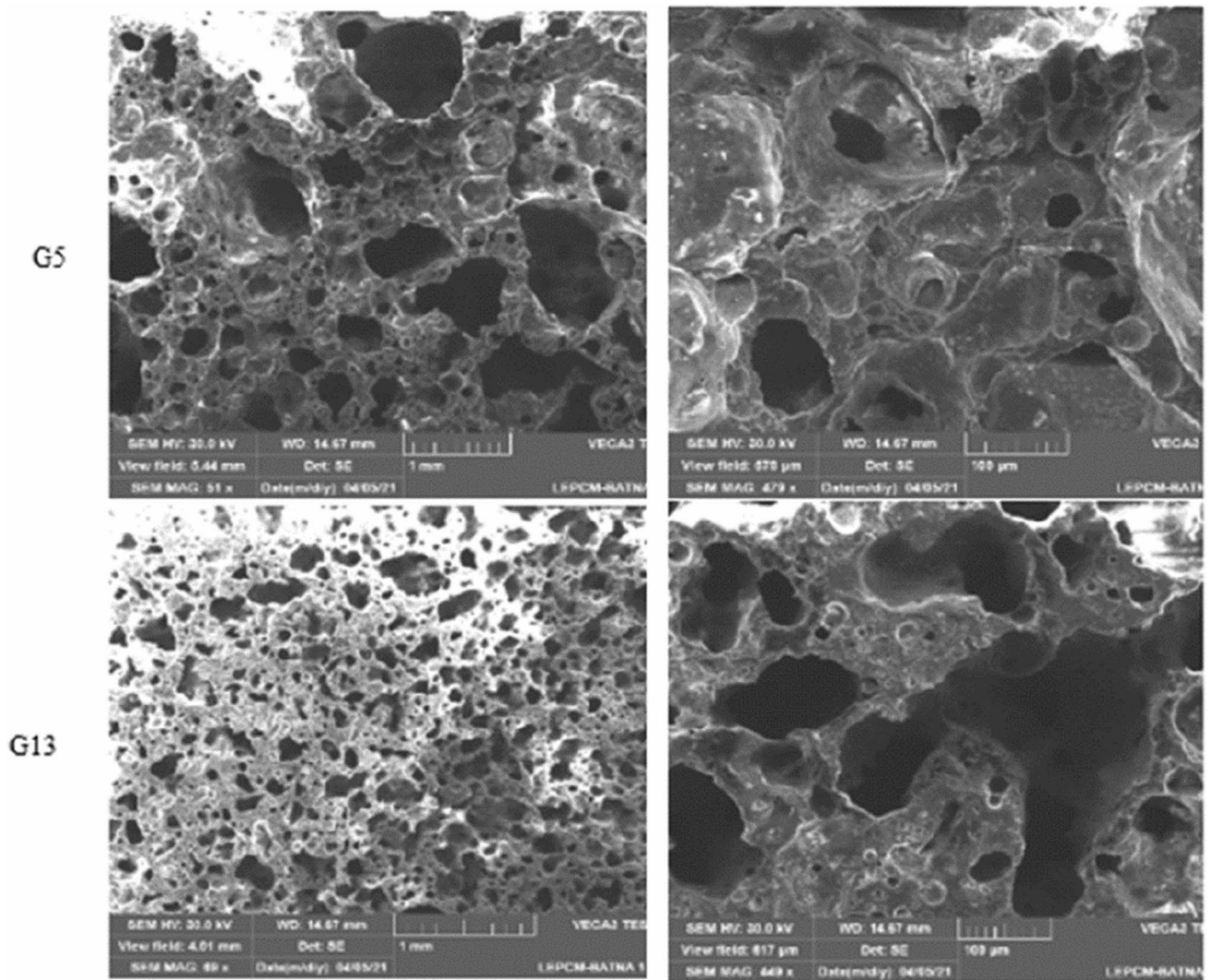
Fig. 11 SEM images of samples foamed with different concentrations of red soil, sintered at 750 °C for 60 min

Figure 9 shows the XRD of the samples with different added amounts of natural red soil fired at 750 °C and 800 °C. The main peaks are assigned to the crystalline phases of quartz (JCPDS 03–065-0466) (JCPDS 01–081-0068), cristobalite (01–076-0938), and devitrite (JCPDS 01–077-0410). Crystalline silica still occurs as a primary crystal phase derived from undissolved quartz. Devitrite (sodium-calcium silicate) is a common devitrification product in soda-lime-silica glass manufacturing. Crystallization experiments on soda-lime glass reveal that devitrite is generated at 750–925 °C and cristobalite at 665–925 °C, in the air atmosphere [39, 40].

Form Fig. 9a, the glass foam containing 5 wt.% of RS had two major crystalline phases identified as cristobalite and quartz with the presence of traces of sodium-calcium silicate; the highest growth of cristobalite (SiO_2) and quartz (SiO_2) is due to the high SiO_2 content. With the addition of

a large quantity of carbonate, the intensity of the cristobalite slightly decreased, accompanied by the appearance of a peak of the combeite phase. In contrast, the intensity of the peaks corresponding to sodium calcium silicate increased. Meanwhile, due to the presence of $CaCO_3$, which may serve as nucleation sites in our glass and inducer of the crystallization process, the high foaming agent content favored the growth of devitrite. The formation of crystalline phases depends on starting composition and time of heat treatment. As shown in Fig. 9b, a dissimilarity in the intensity of the peaks with the variation of heat treatment can be observed. This implies that the crystalline phases are formed, and their amplitude is affected. In both sintering temperatures, the crystalline quartz (SiO_2) and calcium sodium silicate ($Na_2Ca_3Si_6O_{16}$) phases were identified in the XRD patterns. By increasing the sintering temperature from 750 °C to 800 °C, the

prominent new cristobalite (SiO_2) phase (which is a polymorphic phase of quartz) is present after the devitrification of the soda-lime glasses [39].

Microstructural analysis

Figure 10 shows the microstructural changes of glass foams produced with various red soil (RS) content at different temperatures with a holding time of 60 min. It is observed that the pores of foam ceramics are distributed in different forms: open structures with interconnected pores and closed with isolated or mixed pores, with considerably varying sizes. At similar heat treatment, increasing the amount of carbonate from 5 (wt.%) to 16 (wt.%) gradually makes the cell size smaller. Many gaseous products are produced during this time, and an intense gas release escapes from the cells. As can be seen, the foam glass made at 850 °C has an inhomogeneous microstructure with the size of a large cell, the contact area between the initial component (glass and the foaming agent) becomes greater, and the sintering process proceeds faster. In this state, the pores begin close to each other with an increase in the number of channels connecting the pore, which favors the coalescences thermodynamically driven by a decrease in surface energy [7, 41]. However, at low heat treatment (750 °C), the decomposition rate of $CaCO_3$ is lower with a smaller release of gas. Thus, the microstructure of the pore appears uniform with a small size. These images confirm the good correlations between the microstructural study and the evolution of physical and mechanical properties mentioned above.

SEM micrographs illustrated in Fig. 11 consolidate the optical observation. The pores with a wide range of sizes (10–1000 μm) are mostly interconnected and display a relatively inhomogeneous structure. They were formed by the bubbling and coalescence of the bubbles. For all treatments, their dimensions shrank as red soil concentration increased from 5 (wt.%) to 16 (wt.%). In the flowing glassy phase "coalescence," gas production raises the internal pore pressure, balancing the atmosphere pressure and connecting the pores. But in our case, increasing red sol content promotes crystallization and constructs a solid skeleton. Also, it enhances the viscosity of the glass and then traps the gases in tiny circular cells.

Conclusions

This study suggests the feasibility of using a mixture of raw powder (green glass bottle cullet) and abundant natural red soil (5–16 wt.%) as a foaming agent to produce highly porous materials with excellent properties comparable to those of commercial products, prepared with physical foaming approach at a relatively lower temperature. The red soil proved to be a good solid material with remarkable properties for environmental protection. The best physical and mechanical property combinations were obtained for ceramic-glass foams fired at 800 °C in the 30–120 min holding time range. For this case, bulk density varies from 0.26 to 0.75 g·cm^{-3}, while the porosity and compressive strength vary between 70 and 90% and from 1.2 to 6.1 MPa, respectively. The holding time and red soil content are the main factors influencing pore morphology and size. The sintering temperature also has a significant impact on the ceramic-foam glass. In terms of structural properties, it was suggested that increasing the foaming agent content and decreasing the heat treatment time led to a greater number of pores caused by the crystallization process and the highest content of crystalline phases, such as devitrite.

The achieved foams exhibited an excellent strength-to-density ratio (specific strength > 4 (MPa cm^3/g)), which is close to that of a commercial product. Furthermore, the samples obtained in this work are strong candidates for industrial application at a lower cost. Depending on the type of porous structure, it is recommended that porous materials with isolated and closed porosity can be recycled for insulation materials.

Declarations

References

1. Bourhis, E.L.: Glass mechanics and technology, 2nd edn. Wiley (2007)
2. Chinnam, R.K., Francis, A.A., Will, J., Bernardo, E., Boccaccini, A.R.: J. Non. Cryst. Solids **365**, 63 (2013)
3. Silva, R.V., de Brito, J., Lye, C.Q., Dhir, R.K.: J. Clean. Prod. **167**, 346 (2017)

4. Lu, J.X., Poon, C.S.: New trends in eco-efficient and recycled concrete recycling of waste glass in construction materials, pp. 153–167. Elsevier, Amsterdam (2018)

5. Vaisman, Y.I., Ketov, A.A., Ketov, P.A.: Glas. Phys. Chem. **41**, 157 (2015)

6. Bernardo, E., Cedro, R., Florean, M., Hreglich, S.: Reutilization and stabilization of wastes by the production of glass foams. Ceram. Int. **33**(6), 963–968 (2007)

7. Scarinci, G., Brusatin, G., Bernardo, E.: Cell. Ceram. Struct. Manuf. Prop. Appl. pp. 158–176 (2006)

8. Zhu, M., Ji, R., Li, Z., Wang, H., Liu, L.L., Zhang, Z.: Constr. Build. Mater. **112**, 398 (2016)

9. Rincón, A., Giacomello, G., Pasetto, M., Bernardo, E.: J. Eur. Ceram. Soc. **37**, 2227 (2017)

10. Chen, Q., Baino, F., Spriano, S., Pugno, N.M., Vitale-Brovarone, C.: J. Eur. Ceram. Soc. **34**, 2663 (2014)

11. Petersen, R.R., König, J., Smedskiaer, M.M., Yue, Y.: Glas. Technol. Eur. J. Glas. Sci. Technol. Part A **55**, 1 (2014)

12. Bai, J., Yang, X., Xu, S., Jing, W., Yang, J.: Mater. Lett. **136**, 52 (2014)

13. dos Santos, P.A.M., Priebbnow, A.V., Arcaro, S., da Silva, R.M., Lopez, D.A.R., and Rodriguez, A.D.A.L.: Mater. Res. **22**, 0 (2018)

14. Arcaro, S., De Oliveira Maia, B.G., Souza, M.T., Cesconeto, F.R., Granados, L., De Oliveira, A.P.N.: Mater. Res. **19**, 1064 (2016)

15. Saparuddin, D.I., Zaid, M.H.M., Ab Aziz, S.H., Matori, K.A.: Appl. Sci. **10**, 5404 (2020)

16. Ji, R., Zheng, Y., Zou, Z., Chen, Z., Wei, S., Jin, X.: M. Zhang **215**, 623 (2019)

17. Fernandes, H.R., Ferreira, D.D., Andreola, F., Lancellotti, I., Barbieri, L., Ferreira, J.M.F.: Ceram. Int. **40**, 13371 (2014)

18. Llaudis, A.S., Tari, M.J.O., Ten, F.J.G., Bernardo, E., Colombo, P.: Ceram. Int. **35**, 1953 (2009)

19. Tulyaganov, D.U., Fernandes, H.R., Agathopoulos, S., Ferreira, J.M.F.: J. Porous Mater. **13**, 133 (2006)

20. Scheffler, M., Colombo, P.: Cellular ceramics : structure, manufacturing, properties and applications. Wiley-VCH Verlag, Weinheim Germany (2005)

21. Guemache, M.A., Chatelain, J.L., Machane, D., Benahmed, S., Djadia, L.: J. African Earth Sci. **59**, 349 (2011)

22. Chikhi, N., Houari, H.: Sci. Technol. B, Sci. l'ingénieur **0**, 103 (2004)

23. Boulmaiz, B., Benzagouta, M.S.: Les Dolomies des Monts d'Aïn M'lila. Cas du Dj. Teioualt (2017)

24. Traoré, K., Kabré, T.S., Blanchart, P.: Ceram. Int. **29**, 377 (2003)

25. Trindade, M.J., Dias, M.I., Coroado, J., Rocha, F.: Appl. Clay Sci. **42**, 345 (2009)

26. Souza, M.T., Maia, B.G.O., Teixeira, L.B., de Oliveira, K.G., Teixeira, A.H.B., Novaes de Oliveira, A.P.: Process Saf. Environ. Prot. **111**, 60 (2017)

27. Mugoni, C., Montorsi, M., Siligardi, C., Andreola, F., Lancellotti, I., Bernardo, E., Barbieri, L.: Ceram. Int. **41**, 3400 (2015)

28. Fernandes, H.R., Gaddam, A., Tulyaganov, D.U., Ferreira, J.M.F.: Int. J. Appl. Ceram. Technol. **17**, 64 (2020)

29. Teixeira, L.B., Fernandes, V.K., Maia, B.G.O., Arcaro, S., de Oliveira, A.P.N.: Ceram. Int. **43**, 6730 (2017)

30. Hasanuzzaman, M., Rafferty, A., Sajjia, M., Olabi, A.G.: Properties of glass materials. Reference Module in Materials Science and Materials Engineering, pp. 647–657. (2016)

31. Fulcher, G.S.: Am. Ceram. Soc. **8**, 339 (1925)

32. Gibson, L.J., Ashby, M.F.: Cellular solids :structure and properties, 2nd edn. Cambridg Press University, Cambridge, UK (2014)

33. Qu, Y.N., Huo, W.L., Xi, X.Q., Gan, K., Ma, N., Hou, B.Z., Su, Z.G., Yang, J.L.: J. Porous Mater. **23**, 1451 (2016)

34. Qu, Y., Xu, J., Su, Z., Ma, N., Zhang, X., Xi, X., Yang.: Lightweight and high-strength glass foams prepared by a novel green spheres hollowing technique. Ceram. Int. **42**, 2370 (2016)

35. Attila, Y., Güden, M., Taşdemirci, A.: Ceram. Int. **39**, 5869 (2013)

36. Bernardo, E., Scarinci, G., Bertuzzi, P., Ercole, P., Ramon, L., Porous, J.: Mater. **17**, 359 (2010)

37. Monich, P.R., Romero, A.R., Rambaldi, E., Bernardo, E.: Constr. Build. Mater. **261**, 119971 (2020)

38. Ramteke, D.D., Hujova, M., Kraxner, J., Galusek, D., Romero, A.R., Falcone, R., Bernardo, E.: J. Clean. Prod. **278**, 123985 (2001)

39. Zanotto, E.D.: J. Non. Cryst. Solids **129**, 183 (1991)

40. Eubener, J., Brückner, R., Hessenkemper, H.: Glas. Berichte. **65**, 256 (1992)

41. Pokorny, A., Vicenzi, J., Pérez Bergmann, C.: Waste Manag. Res. **29**, 172 (2011)